Eng. Sci., 2025, **36**, 1676

Engineered Science
DOI: https://dx.doi.org/10.30919/es1676

Nacre Inspired Silicon Carbide Whiskers Embedded Bilayer Hydrothermal Carbon Interphase for Strengthening Carbon Fiber-Reinforced Zirconium Boride - Silicon Carbide Composites

Jiayin Zhao,[1] Huan Yang,[1] Xia Zhang,[1] Xiaoyi Jiang,[1] Ying Bao,[2, 3] Mingyu Yao,[1] Feilong Huang[1] and Cheng Fang[1,*]

Abstract

Inspired by the mineral bridge mechanism in nacreous architectures, this study proposes a novel interface design aimed at enhancing the comprehensive mechanical properties of carbon fiber-reinforced Zirconium boride - Silicon carbide composites. Silicon carbide whiskers (SiC_w) were incorporated as structural bridges between bilayer hydrothermal carbon coatings (HTCC), leading to the successful construction of a hierarchical HTCC-SiC_w-HTCC (HS_wH) interphase via stepwise hydrothermal synthesis. The SiC_w bridges not only strengthened the interlayer bonding but also maintained controlled interfacial slippage, achieving a synergistic balance between efficient load transfer and energy dissipation. Mechanical characterization demonstrated that the HS_wH-modified composites exhibited significantly enhanced flexural strength (318 ± 37 MPa) while retaining high fracture toughness (7.36 ± 0.91 MPa·$m^{1/2}$), surpassing the performance of conventional bilayer HTCC systems. Additionally, thermal shock resistance was markedly improved, with critical failure temperatures reaching 908 ℃ for the optimized composite. This work presents a biomimetic strategy for designing high-performance interfaces in carbon fiber toughened ceramic matrix composites.

Keywords: Carbon fiber toughened ceramic matrix composites; Biomimetic interface; Hydrothermal carbon coating.
Received: 15 May 2025; Revised: 17 June 2025; Accepted: 29 July 2025.
Article type: Research article.

1. Introduction

Carbon fiber, characterized by its remarkable mechanical properties like extremely high tensile strength, has been recognized as the preferred reinforcement for ultra-high temperature ceramics (UHTCs).[1,2] Among diverse composite systems, carbon fiber-reinforced ZrB_2-SiC composites (C_f/ZrB_2-SiC) have been widely applied in thermal protection systems for hypersonic vehicles because of their outstanding high-temperature mechanical performance and oxidation resistance.[3-5] Nevertheless, the composite encounters critical challenges during high-temperature sintering processes. Carbon fibers are prone to undergo interfacial reactions with oxide species (*e.g.*, ZrO_2) on the surfaces of ceramic particles, which not only result in the structural degradation of fibers but also give rise to overly strong interfacial bonding.[6] Such strongly bonded interfaces considerably enhance the susceptibility of fibers to matrix crack propagation, suppressing critical toughening mechanisms such as fiber pull-out and bridging, and ultimately leading to a significant reduction in the composite's fracture toughness.[7] Therefore, precise regulation of the fiber/matrix interfacial bonding strength through interface modification has become crucial for optimizing the performance of the composite.

Silicon carbide (SiC) and Boron nitride (BN) coatings exhibit superior oxidation resistance and can be deposited onto the surface of carbon fibers via the chemical vapor deposition (CVD) process.[8,9] However, the thermal stress mismatch between these ceramic coatings and carbon fibers often results in coating cracking and delamination, which may subsequently induce fiber fracture. The preparation of carbon material coatings with a structure analogous to that of carbon fibers is considered a more advantageous approach. Zhang et al. conducted a comparative study on C_f/ZrB_2-SiC materials with and without carbon coatings, revealing that the incorporation of carbon coatings significantly enhanced the

[1] *School of Materials Science and Engineering, Zhengzhou University, Zhengzhou 450001, China*
[2] *School of Mechanical Engineering, Henan University of Engineering, Zhengzhou, 451191, China*
[3] *Anhui Hengli Additive Manufacturing Technology Co., Ltd., Wuhu 241000, China*
**Email:* fangcheng@zzu.edu.cn (Cheng Fang)

fracture toughness of the materials.[10] The fracture mode transitioned from brittle to non-brittle, and the fracture energy increased by a factor of four. Cheng *et al*. fabricated C_f/ZrC-SiC composites using the slip casting method, where the carbon coating improved the interfacial bonding between the fibers and the matrix, thereby enhancing the fracture toughness and fracture energy of the material.[11] Therefore, carbon materials represent an ideal choice for surface coatings in carbon fiber-reinforced ultra-high-temperature ceramic systems.

Pyrolytic carbon (PyC) coatings, which exhibit a unique layered structure and anisotropic properties, can be deposited on the surface of carbon fibers via the CVD technique.[12,13] However, conventional PyC coating processes have difficulty in achieving the regulation of the fiber/coating interfacial strength through basic deposition parameters such as processing time and temperature. To overcome these limitations, hydrothermal carbon coatings (HTCCs) derived from hydrothermal carbonization (HTC) technology have emerged as a novel interfacial engineering approach. This process utilizes glucose precursors to achieve uniform fiber coating under hydrothermal conditions.[14] Importantly, the controllable volumetric shrinkage during the subsequent carbonization shows a functional dependence on the coating thickness, providing new opportunities for the regulation of interfacial strength.[15] By constructing bilayer or multilayer HTCC architectures, graded crack deflection can be realized through crack branching-induced energy dissipation, significantly enhancing the fracture energy of the composite.[16] Nevertheless, our previous study indicated that excessive shrinkage might result in micrometer-scale interfacial gaps between the outer and inner layer HTCCs, undermining the load transfer efficiency at the interface and ultimately restricting the flexural strength of the composite.[17] This phenomenon discloses the inherent contradiction in attaining a balanced strengthening and toughening mechanism through single-phase coating interphase.

The establishment of structural bridges among lamellar materials can enhance interlayer interactions. A representative case can be seen in shell nacre. It exhibits a layered microstructure, primarily consisting of 95% hard calcium carbonate lamellae interconnected by 5% organic material forming mineral bridges.[18] Mineral bridges serve as the critical structures connecting individual calcium carbonate layers, thereby enabling the fracture toughness of nacre to surpass that of single-phase aragonite by a factor of three to nine.[19,20] By enhancing interfacial friction between calcium carbonate layers and effectively inhibiting crack propagation along straight paths, the mineral bridges play a pivotal role in significantly elevating the overall mechanical performance of nacre.[21] Inspired by this biological design, the introduction of bridging materials within bilayer HTCC interfaces has the potential to achieve similar optimization effects. The key challenges reside in the selection of bridging materials and their effective integration between HTCCs.[22] Silicon carbide whiskers (SiC_w) display an optimal combination of thermomechanical properties, such as a high melting point, low density, exceptional tensile strength, and high elastic modulus, making them ideal for high-temperature interface engineering.[23,24]

Based on this strategy, this study developed a novel HTCC-SiC_w-HTCC (HS_wH) interphase architecture via stepwise hydrothermal synthesis, where SiC_w bridges are embedded between bilayer HTCCs. The regulation mechanisms were clarified through the systematic investigation of the effects of SiC_w on the interfacial behavior and macroscopic performance of the C_f/ZrB_2-SiC composites. This bioinspired interface design offers new approaches for achieving strength-toughness synergy in advanced fiber-reinforced UHTC composites.

2. Materials and methods

2.1 Raw materials

Carbon fiber braids (density: 0.48 g/cm^3) were provided by Jiangsu Tianniao High Technology Co., Ltd (China), fabricated through needle-punching technology using the stacking of T700 carbon nonwoven fiber cloth. Chemical reagents for HS_wH interphases synthesis encompassed D-glucose monohydrate ($C_6H_{12}O_6{\cdot}H_2O$, 98%), hydrochloric acid (HCl, 37.5%), and nitric acid (HNO_3, 65%), as well as SiC whiskers (600 nm diameter, 6 μm length, aspect ratio ≈ 10), all of which were obtained from Xi'an Mingbo Chemical Co., Ltd. Constituent materials for C_f/ZrB_2-SiC fabrication included: ZrB_2 powder (99.5% purity, Beijing HWRK Chem Co., Ltd.), polycarbosilane solution (PCS, Institute of Chemistry, Chinese Academy of Sciences), polyethyleneimine (PEI, Mw = 10000), and polyvinyl butyral (PVB, Mw = 3000) from Aladdin Reagent Co., Ltd.

2.2 Fabrication of HS_wH interphases and C_f/ZrB_2-SiC composites

A two-step synthesis approach was employed to controllably incorporate SiC_w into the interface of a bilayer HTCCs. Silicon carbide whiskers with a specified mass ratio were evenly dispersed in a 20 wt% glucose solution, and a stable suspension was achieved through ultrasonic treatment. The pre-treated carbon fiber fabric was fully impregnated with the suspension and underwent a hydrothermal reaction at 180 ℃ for 6 hours, allowing HTCC co-deposited with silicon carbide whiskers to form a composite structure. Subsequently, the sample was heated in a tube furnace to 1000 ℃ at a rate of 5 ℃/min and maintained for 1 hour to eliminate oxygen-containing functional groups on the HTCC surface, thereby suppressing the strong chemical bonding between the inner and outer coatings during the subsequent hydrothermal deposition. A secondary hydrothermal deposition was carried out on the primary composite coating under the same temperature and duration conditions, with the glucose concentration raised to 30 wt.% to eventually fabricate the HS_wH interphases on carbon fibers. To systematically explore

the influence of the bridging structure on the performance of composites, two comparative groups with glucose to whisker mass ratios of 10:1 and 30:1 were processed, which were respectively designated as F_1 and F_2. A control group of pristine carbon fiber (without whiskers) was designated as F_0. The preparation methods of C_f/ZrB_2-SiC composites can be found in our previous studies.[17] Composite samples prepared by the three types of fibers were respectively named as CZS-0, CZS-1, and CZS-2.

2.3 Characterization and measurement

Composite density measurements were carried out following Archimedes' principle. Microstructural characterization of HTCC-coated fibers was conducted using scanning electron microscopy (SU-70, Hitachi, Japan). X-ray diffraction patterns were acquired using an X-ray diffractometer (XRD, Empyrean, PANalytical B.V., the Netherlands) with Cu Kα radiation. The sample size of flexural strength bar is 36 mm × 4 mm × 3 mm, the span is 30 mm and the loading speed is 0.5 mm/min. Fracture toughness was evaluated using the single-edge notch beam (SENB) method. The specimens had dimensions of 22 mm × 4 mm × 2 mm, with a notch width and depth of 0.2 mm and 2 mm, respectively. The span length for the SENB test was 16 mm, and the loading speed was 0.05 mm/min. The final results were obtained by averaging six calculated values. Nanoscale interfacial behavior was evaluated by fiber push-in testing (Nano Indenter G200, Keysight Technologies, USA). The thermal shock behavior was characterized by the water quenching method.[25,26] Three-point bending testing bars were heated in air and maintained at a certain temperature for 10 minutes. Subsequently, they were directly dropped into a water bath kept at a constant temperature of 25 ℃. The thermal shock temperature difference (ΔT) was set within the range of 600 ℃ to 1400 ℃.

3. Results and discussion

3.1 Effect of HS_wH interphase on mechanical properties of C_f/ZrB_2-SiC composites

As shown in Fig. 1, the pristine fiber F_0 presented a smooth surface morphology without discernible grooves, while the modified samples exhibited significant morphological differences. Sparse SiC_w were distributed over the F_1 surface, while F_2 showed densely populated SiC_w due to the higher whisker content in the hydrothermal system. The morphological analysis indicated that SiC_w were partially embedded within the inner HTCC layer. The exposed extremities could form “bridges” to connect this HTCC layer and the next outer HTCC layer.

A secondary hydrothermal process was employed to construct HTCC coatings on the HTCC-SiC_w framework, ultimately synthesizing the HS_wH interface. It is important to note that the SiC_w content was constrained to the CZS-2 level (with a mass ratio of glucose to SiC_w within 10:1) due to the inherent dispersion limitation. When the ratio increased to 5:1 in the hydrothermal glucose solution, van der Waals force-driven agglomeration of whiskers surpassed the electrostatic stability threshold, resulting in the formation of numerous SiC_w clusters. As a consequence, the resultant HTCC coating exhibited poor uniformity and a high density of cracks, as illustrated in Fig. S1. Surface structural analysis of the modified fibers (Fig. 2) revealed that the initial HTCC-SiC_w architecture was entirely encapsulated by the outer HTCC layer. Pronounced protrusions were observed on the outermost surface in regions where whiskers exhibited a near-perpendicular orientation. These protrusions promoted the formation of interlocking structures between fibers and the ceramic matrix, thereby enhancing load transfer efficiency from the matrix to the fibers.[27]

After the establishment of HS_wH interfaces on carbon fibers, C_f/ZrB_2-SiC composites were fabricated by means of slurry injection combined with precursor impregnation and pyrolysis (PIP). Twelve PIP cycles resulted in composite densification exceeding 80%, and the corresponding densification kinetics is depicted in Fig. S2. CZS-0, CZS-1, and CZS-2 showed minimal density variations (< 3% range), effectively minimizing the interference from density variations in evaluating the impact of interface characteristics on composite properties. Representative cross-sectional SEM images and the corresponding elemental distribution of the different composites are presented in Fig. 3. The prepared

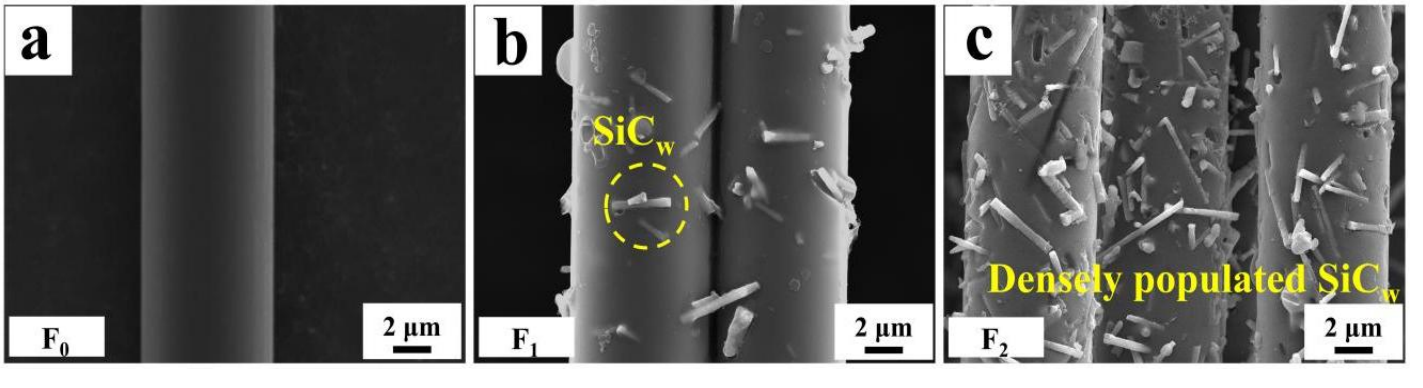

Fig. 1: Morphology of HTCC-SiC_w coating on carbon fibers: (a) F0; (b) F1; (c) F2.

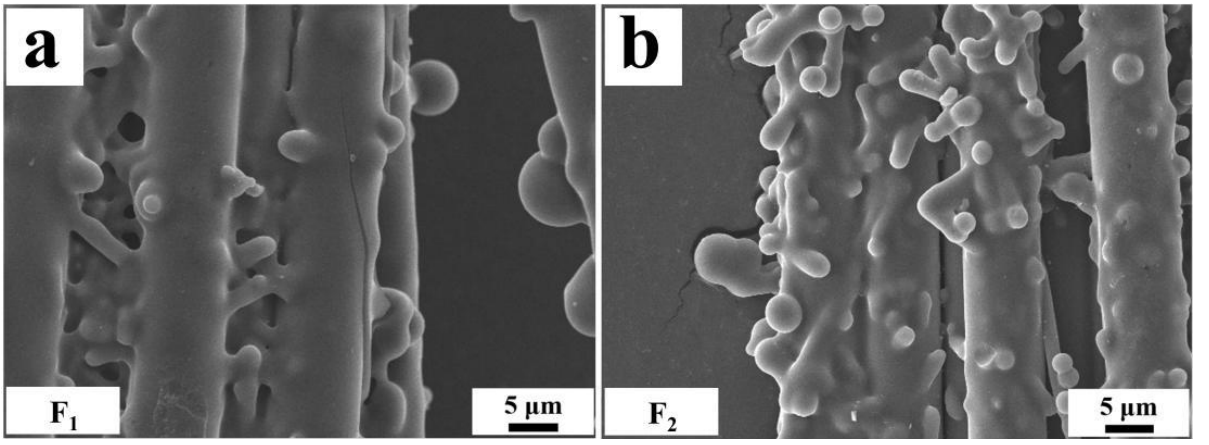

Fig. 2: Interface morphology of HS_wH on carbon fibers: (a) F_1; (b) F_2.

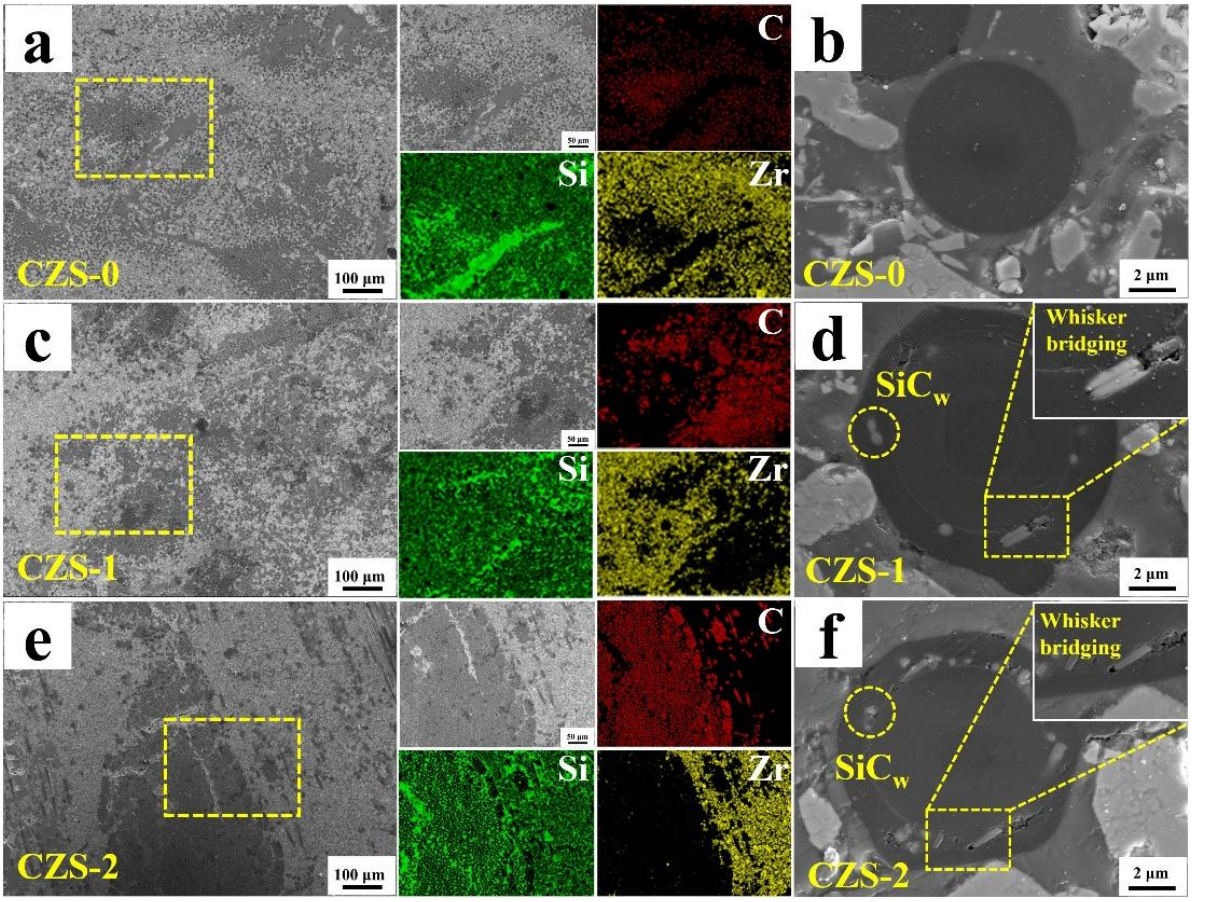

Fig. 3: Microstructural characteristics and corresponding elemental distribution of the composites: (a-b) CZS-0; (c-d) CZS-1; (e-f) CZS-2.

composites exhibit relatively high overall density, with no evident presence of large pores. Furthermore, the densities of the three composite materials are found to be nearly identical, which is in excellent agreement with the density data presented in Fig. S2. The XRD patterns presented in Fig. S3 and EDS analysis in Fig. 3 confirm that the composites consist of ZrB_2, SiC and carbon fibers. Moreover, the fiber bundles within the fiber-woven body exhibit excellent impregnation. Fig. 3b shows the amplified microstructure of the CZS-0 composite, revealing continuous and gapless interfaces between uncoated carbon fibers and the ceramic matrix. The phenomenon was consistently demonstrated in our previous studies.[17] This strong interfacial bonding resulting from direct fiber-matrix contact promotes the stress concentration effect at interfaces, which constitutes the primary mechanism for fiber brittle fracture during composite loading.[28] Figs. 3d and 3f illustrate the successful fabrication of bilayer HTCCs as fiber/matrix transition layers, with interlayer bridge connections established via SiC_w.

Mechanical performances of the three composites are presented in Fig. 4a. The CZS samples demonstrated flexural strength and fracture toughness values of 182 ± 39 MPa and

3.23 ± 0.56 MPa·m$^{1/2}$, respectively. Previous studies indicated that bilayer coatings could enhance composite toughness through interfacial stress redistribution mechanisms,[29] attaining maximum values up to 8.25 ± 0.82 MPa·m$^{1/2}$. Nevertheless, their flexural strength was still suboptimal (215 ± 24 MPa). To date, hardly any composites optimized by HTCC have demonstrated a bending strength exceeding 300 MPa in published studies (shown in Fig. 4c and Table S1).[16,17,30,31] This limitation mainly stemmed from interfacial gaps within bilayer coatings that undermined load transfer efficiency. The incorporation of SiC_w significantly improved flexural strength, with CZS-1 and CZS-2 reaching 231 ± 38 MPa and 318 ± 37 MPa, respectively. This enhancement verified the effectiveness of SiC_w bridging structures in optimizing load transfer across bilayer hydrothermal carbon interfaces. Crucially, the fracture toughness of CZS-2 remained at 7.36 ± 0.91 MPa·m$^{1/2}$, indicating that the bridging architecture offered sufficient interfacial slippage capacity to prevent brittle fiber failure while maintaining the toughness of the composite. The load-displacement curve of CZS-0 composite material shows pseudoplastic fracture characteristics (Fig. 4b). Nevertheless, in the load-displacement curve of CZS-2, "pop-in" events occur frequently (sudden stress drop followed by rapid recovery). The phenomena signify the retained integrity of the CZS-2 under high stress conditions and the delayed catastrophic failure. The emergence of "pop-in" behavior is directly related to the enhanced crack deflection capability at SiC_w-modified interfaces, representing a major contributor to the observed mechanical improvements.[32] Notably, partial detachment of SiC_w during the composite fabrication process was observed in Fig. S4. Nevertheless, previous studies have confirmed that SiC_w can still contribute to a moderate enhancement of the mechanical properties in such composite systems.[33] Fig. S5 displays the morphologies of crack propagation zone for the three composites. Multiple toughening mechanisms including fiber bridging, crack deflection, and fiber pull-out were witnessed in CZS-1 and CZS-2. The zigzag crack propagation path further enhances energy dissipation during the fracture process, which is also one of the primary factors contributing to the "pop-out" events in the load-displacement curve (Fig. 4b).[34,35]

Fracture morphology analysis in Fig. 5 reveals distinct failure characteristics among the composites. The fracture surfaces of carbon fibers in CZS-0 aligned nearly flush with the matrix, indicating strong fiber/matrix bonding through

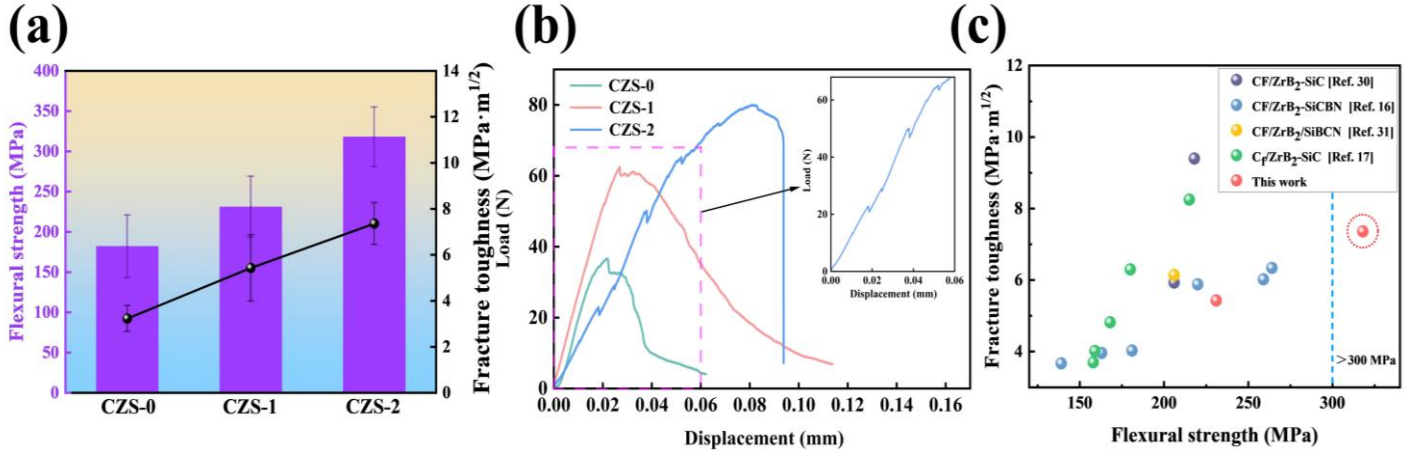

Fig. 4: (a) Mechanical properties of different composites; (b) Load-displacement curves of different composite materials; (c) Performance statistics of C_f/UHTCs composites optimized by HTCC interface.

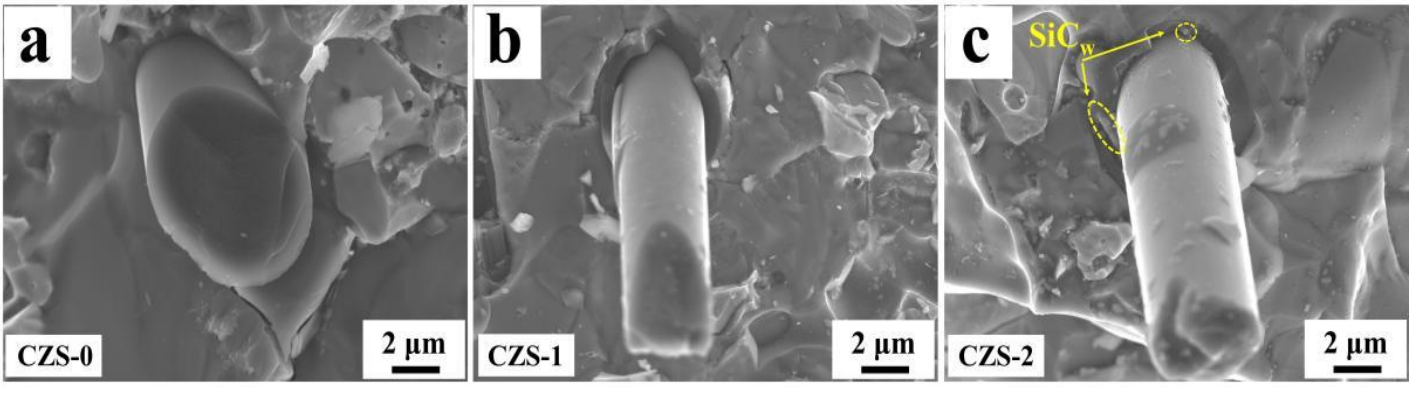

Fig. 5: Fracture morphology of different composites: (a) CZS-0; (b) CZS-1; (c) CZS-2.

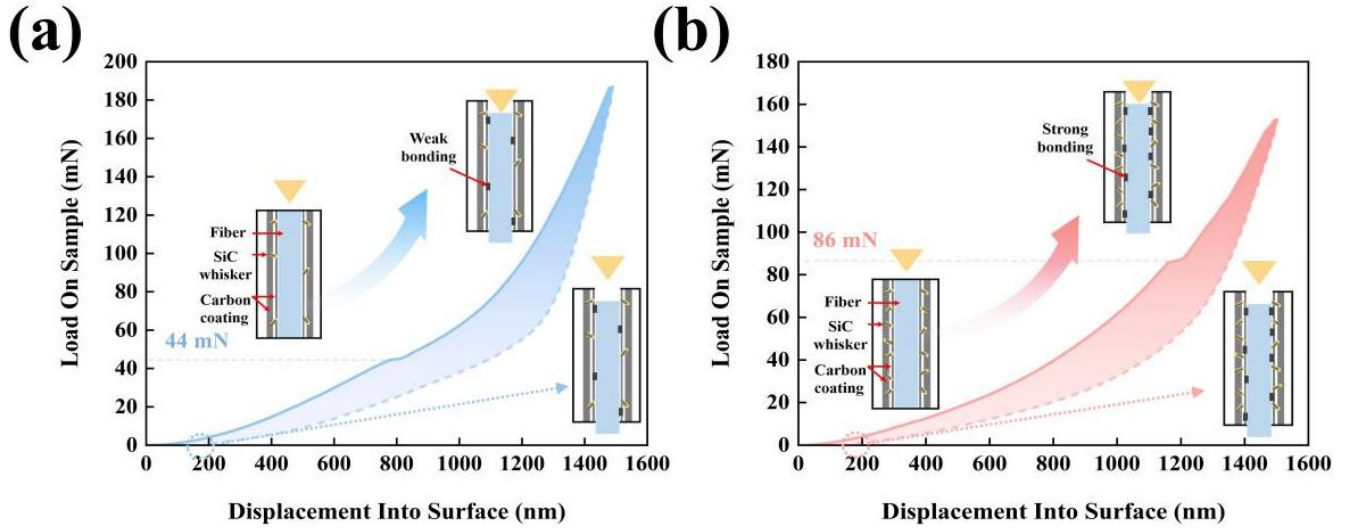

Fig. 6: Load-displacement curves of fiber pull-out test in composites: (a) CZS-1; (b) CZS-2.

interfacial reactions (Fig. 5a). Conversely, CZS-1 (Fig. 5b) and CZS-2 (Fig. 5c) exhibited distinctly elongated fiber pull-out lengths. This primarily demonstrates the interfacial stress redistribution capability of bilayer HTCC coatings, consistent with verification from out prior investigations.[17] CZS-1 and CZS-2 displayed near-planar fracture surfaces across their bilayer coatings, contrasting with conventional bilayer-coated composites that exhibit stepwise pull-out morphology accompanied by interlayer crack propagation.[36,37] This morphological distinction arises from enhanced interlayer connectivity induced by SiC_w. Some SiC_w could be identified in the interface regions (Fig. 5c), further validating this interfacial reinforcement mechanism.

3.2 Toughening mechanism of HS_wH interphase in C_f/ZrB_2-SiC composites

Interfacial debonding forces were measured using single fiber push in tests with a triangular indenter. The maximum indentation depth was set at 1.5 μm to avoid contact between the indenter and ceramic matrix. Previous studies have characterized the interfacial properties of composites with the same HTCC structure.[17] Uncoated fibers showed critical debonding loads over 200 mN, while bilayer HTCCs matching the structure design in this study reduced this value to 16 mN. Based on these established results, this study specifically analyzed the interfacial friction properties of two composites incorporating SiC_w between bilayer HTCCs. Fig. 6 shows the load displacement curves of CZS-1 and CZS-2 during fiber push in tests. Both composites exhibited curves with transition points, indicating slight slippage between fibers and the matrix. The loads corresponding to these slippage points reflect interfacial friction forces. CZS-1 displayed a critical debonding load of 44 mN. This demonstrates that the bridging structures formed by SiC_w between bilayer hydrothermal carbon coatings increased interlayer friction, thereby enhancing interfacial bonding strength.[38,39] The friction further increased with the higher SiC_w content, as shown by the elevated critical debonding load of 86 mN for CZS-1. These results confirm that SiC_w effectively strengthen interfacial bonding in bilayer HTCC systems. Fig. S6 clearly depicts the interfacial morphology before and after testing. Partial SiC_w protrusion was observed at the interface, indicating that SiC_w have been applied stresses during the extrusion process. When interfacial bonding strength proves insufficient to fully counteract external loads, stress release occurs through SiC_w slippage or fracture, thereby delaying interfacial debonding progression. These observations further confirm the critical role of SiC_w in regulating interfacial bonding strength.

The synergistic mechanism between SiC_w and bilayer HTCC in interfacial property regulation is visually illustrated in Fig. 7. In conventional bilayer HTCC-modified composites, carbonization shrinkage of HTCC layers creates microscopic interlayer gaps. These gaps establish weak interfacial connections that promote crack propagation along preferentially weakened paths, effectively dissipating impact energy while preserving carbon fiber integrity. Microstructurally, bilayer HTCC systems typically exhibit non-coplanar fracture surfaces with characteristic “stepwise pull-out”, which have been repeatedly confirmed in prior investigations. Nevertheless, this energy-dissipative architecture inherently limits the load transfer efficiency at the interface, ultimately constraining flexural strength enhancement of the composite. Based on the biomimetic material design concept of biomass nacre, the establishment of structural bridges among lamellar materials can strengthen the interlayer interactions (Fig. 7a). Upon SiC_w incorporation between bilayer coatings, a nacre-like mineral bridge mechanism is established (Fig. 7b). This configuration simultaneously strengthens interlayer bonding while retaining controlled slippage capacity.[40] Therefore, HTCCs in HS_wH interphase exhibit predominantly planar fracture surfaces, whereas the carbon fibers demonstrate retained extended pull-out lengths (Figs. 7c-d). This synergistic configuration enables

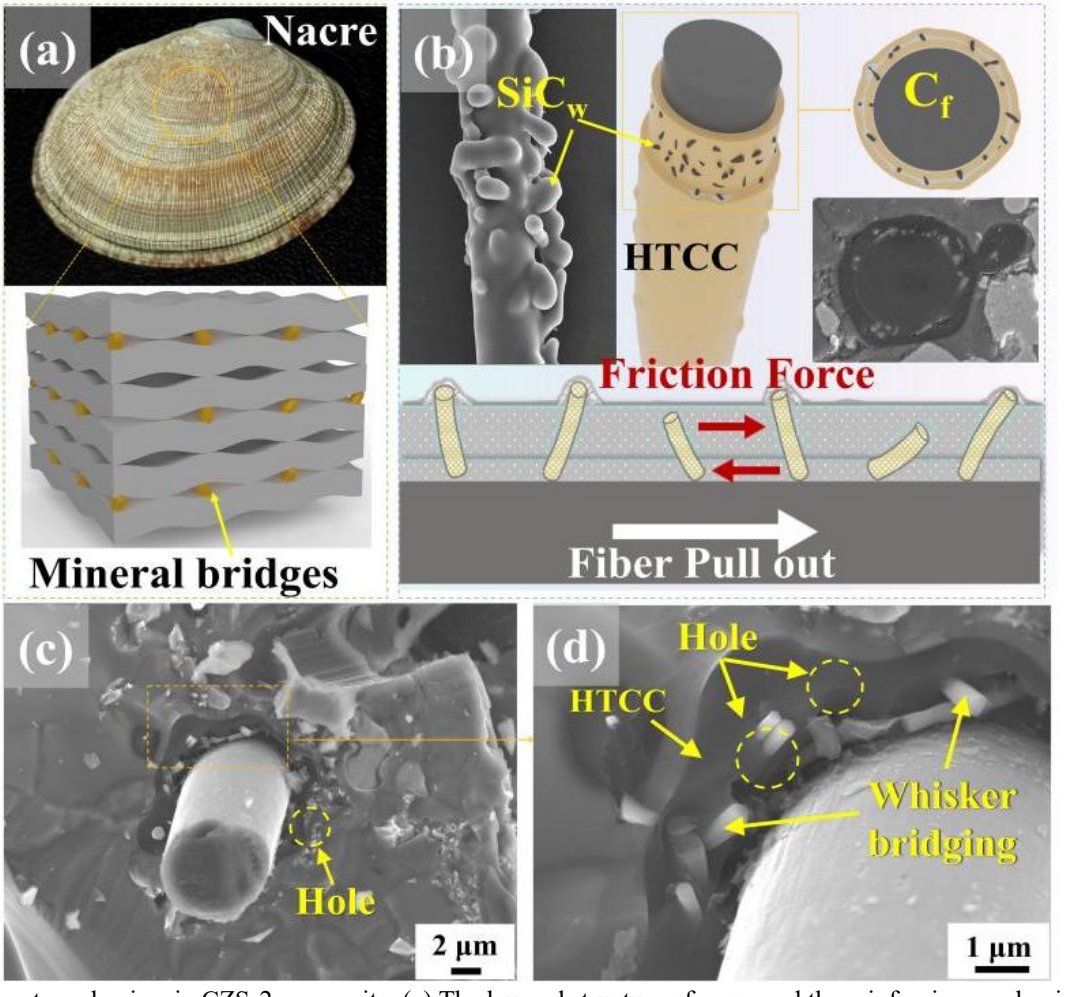

Fig. 7: Reinforcement mechanism in CZS-2 composite: (a) The layered structure of nacre and the reinforcing mechanism of mineral bridges; (b) HS_wH interfacial configuration on carbon fibers with its synergistic enhancement mechanism; (c-d) interfacial bonding characteristics and whisker bridging phenomena in CZS-2.

simultaneous improvement in load transfer efficiency and energy dissipation capacity, ultimately yielding balanced mechanical performance enhancement.

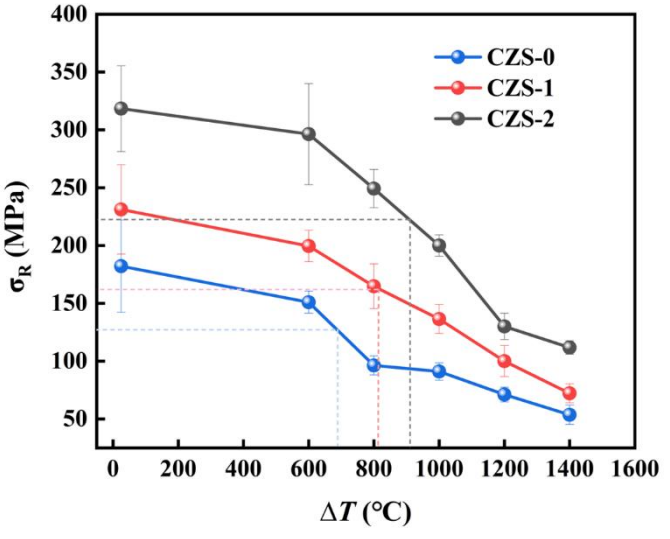

Fig. 8: Residual flexural strength of different composites after thermal shock.

3.3 Effect of HS_wH interphase on thermal shock properties of composites

Interfaces can function as critical stress buffers and thermal stress distributors during thermal shock events. Consequently, the influence of the HS_wH interphase on the thermal shock resistance of composites merits further investigation. Fig. 8 illustrates the temperature-dependent variations in flexural strength of composites after exposure to thermal shock. The calculated critical thermal shock temperature difference (ΔT, 30% strength degradation threshold) were 686 °C, 815 °C, and 908 °C for CZS-0, CZS-1, and CZS-2 composites, respectively. It is noteworthy that non-fiber-toughened ZrB_2-SiC ceramics typically exhibit ΔT values not exceeding 700 °C. The incorporation of carbon fiber reinforcement effectively enhances damage tolerance and thermal shock resistance. However, literature indicates that most carbon fiber-reinforced ZrB_2-SiC composites lacking interface optimization generally have ΔT values below 900°C. Detailed data statistics are listed in Table S2. However, the CZS-2 composite with the SiC_w-bridged interphase demonstrates a substantial improvement in ΔT, reaching 908°C. This represents a 32.4% enhancement over the non-optimized composite (686 °C) within this work

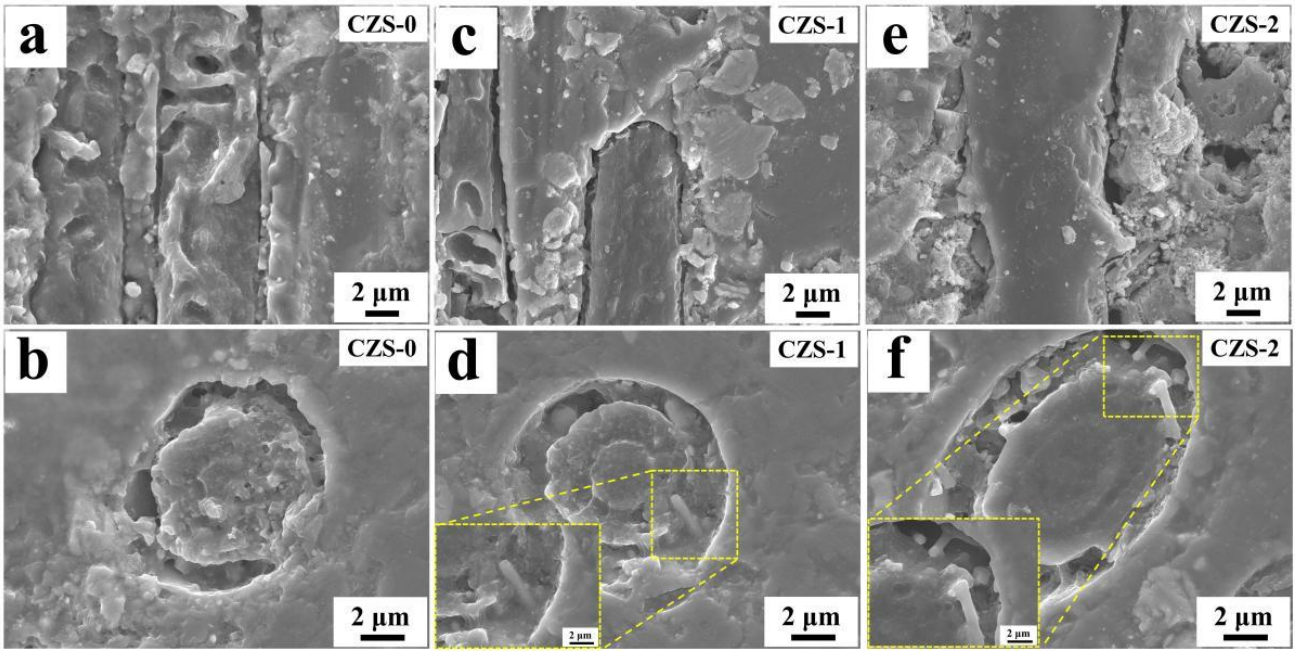

Fig. 9: The surface morphology of different composites after thermal shock at 800 °C: (a-b) CZS-0; (c-d) CZS-1; (e-f) CZS-2.

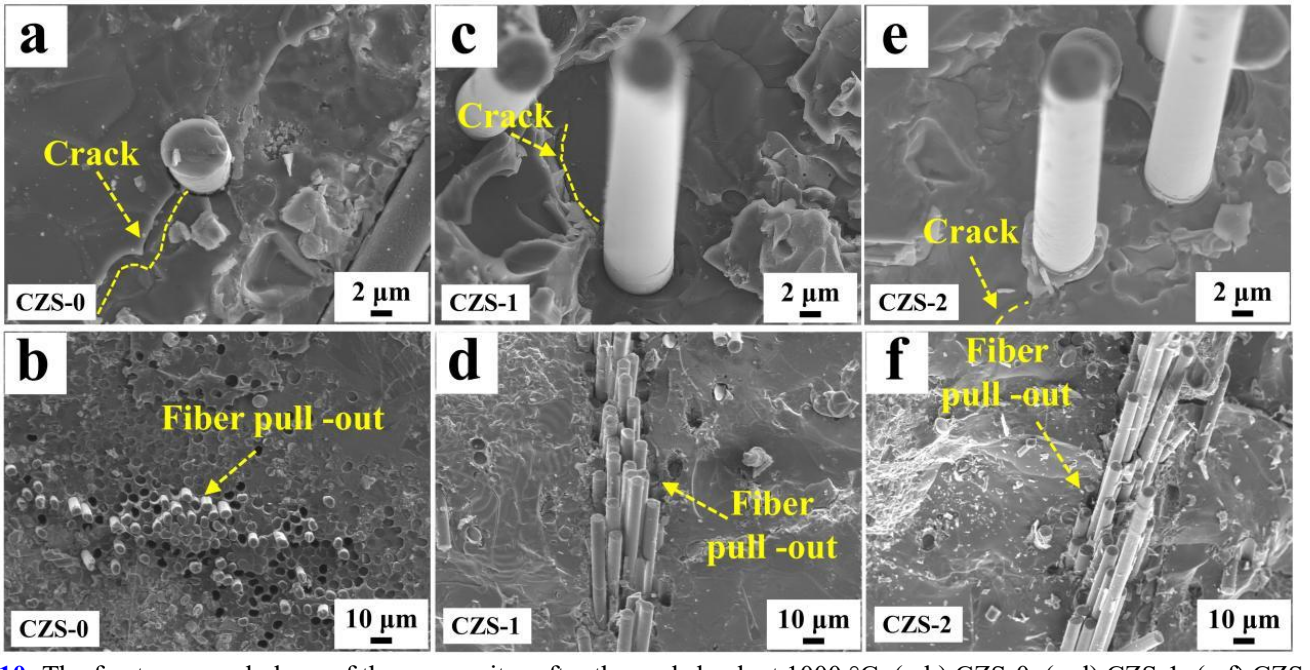

Fig. 10: The fracture morphology of the composites after thermal shock at 1000 °C: (a-b) CZS-0; (c-d) CZS-1; (e-f) CZS-2.

and surpasses the performance of typical unoptimized systems reported in the literature. These results clearly validate the high effectiveness of the interface optimization strategy in enhancing the thermal shock resistance of C_f/ZrB_2-SiC composites.

Microstructural analysis provides critical insights into the enhanced thermal shock resistance. Fig. 9 shows the surface morphological characteristics of composites after 800 °C thermal shock. Surfaces typically suffered severe oxidative damage due to direct air exposure. The carbon fibers in CZS-0 exhibited pronounced degradation features. In contrast, CZS-1 and CZS-2 composites maintained relatively intact carbon fiber structures despite partial oxidation damage to outer coatings under high-temperature conditions. This observation indicates that HS_wH interphase establishes an effective protective barrier isolating carbon fibers from oxidative environments. Figs. 9d and 9f further confirm that SiC_w maintained structural integrity during thermal shock, retaining their reinforcement capability in high-temperature conditions.

Fracture surface morphologies of the composites subjected to thermal shock at 1000 °C are presented in Fig. 10. Internal oxidation was effectively suppressed by the protective ceramic matrix. The CZS-0 composite exhibited interfacial failure characterized by smooth fracture surfaces with negligible fiber pull-out. Localized cracks adjacent to carbon fibers originated

from thermal mismatch stresses induced by the coefficient of thermal expansion discrepancy between carbon fibers (Fig. 10a).[41,42] In contrast, CZS-1 and CZS-2 composites demonstrated pronounced fiber pull-out behavior with average lengths (Figs. 10c-f). This mechanical response confirms the retained toughening functionality of the HS_wH interphase under extreme thermal stress.

4. Conclusion

This study successfully developed a biomimetic HS_wH interphase by integrating SiC_w between bilayer HTCCs, significantly enhancing the comprehensive mechanical performance of carbon fiber-reinforced ZrB_2-SiC composites. SiC_w bridged architecture strengthened interfacial bonding while maintaining effective energy dissipation. The composites exhibited superior flexural strength (up to 318 ± 37 MPa) and thermal shock resistance, with critical failure temperatures reaching 908 °C. Microstructural analysis confirmed the structural integrity of SiC_w under high temperature oxidation environment, effectively mitigating fiber-matrix debonding and crack propagation. This bioinspired interface design strategy provides a scalable solution for advanced ceramic composites in thermal protection systems.

Acknowledgments

This work was supported by the National Natural Science Foundation of China (No. U23A20562, 52172075, 52302074 and 52302066, 52401208), the China Postdoctoral Science Foundation (No. 2021M702931), International Science and Technology Cooperation Program of Henan Province (No. 252102520043), Key Scientific Research Project for Application Study in Colleges and Universities of Henan Province (No. 25A430043), Anhui Postdoctoral Science Foundation (No. 2025C1158).

Conflict of Interest

There is no conflict of interest.

Supporting Information

Applicable.

CRediT Statement

Jiayin Zhao: Data curation, Data visualization, Formal analysis, Methodology, Writing – original draft. Huan Yang: Resources, Data visualization, Writing – review & editing. Xia Zhang: Data curation, Validation, Writing – review & editing. Xiaoyi Jiang: Data curation, Validation. Ying Bao: Supervision, Formal analysis, Methodology. Mingyu Yao: Data curation, Data visualization. Feilong Huang: Conceptualization, Supervision, Writing – review & editing. Cheng Fang: Supervision, Funding acquisition, Writing – review & editing.

References

[1] D. Zhang, P. Hu, S. Dong, X. Liu, C. Wang, Z. Zhang, X. Zhang, Oxidation behavior and ablation mechanism of C_f/ZrB_2-SiC composite fabricated by vibration-assisted slurry impregnation combined with low-temperature hot pressing, *Corrosion Science*, 2019, **161**, 108181, doi: 10.1016/j.corsci.2019.108181.

[2] T. Jing, Y. Xin, L. Zhang, X. Sun, C. He, J. Wang, F. Qin, Application of Carbon Fiber-Reinforced Ceramic Composites in Active Thermal Protection of Advanced Propulsion Systems: A Review, *The Chemical Record*, 2023, **23**, e202300022, doi: 10.1002/tcr.202300022.

[3] Y. Liu, J. Wang, R. Jing, Y. Zhang, Z. Liao, Y. Zu, Enhanced fracture properties of continuous C_f/ZrB_2-based composites with polydopamine-derived carbon boundary layer, *Surfaces and Interfaces*, 2024, **46**, 103925, doi: 10.1016/j.surfin.2024.103925.

[4] Z. Wang, B. Wang, S. Li, X. Jin, X. Zhang, S. Meng, G. Fang, Temperature-dependent oxidation kinetics and mechanical properties degradation of C_f/ZrB_2-SiC composites, *Corrosion Science*, 2023, **224**, 111479, doi: 10.1016/j.corsci.2023.111479.

[5] Y. Liu, Y. Cheng, D. Ma, N. Hu, W. Han, D. Liu, S. Wu, Y. An, A. Wang, Continuous carbon fiber reinforced ZrB_2-SiC composites fabricated by direct ink writing combined with low-temperature hot-pressing, *Journal of the European Ceramic Society*, 2022, **42**, 3699-3707, doi: 10.1016/j.jeurceramsoc.2022.03.045.

[6] D. Zhang, H. Yu, A. Wang, Q. Wang, L. Ren, P. Hu, D. Sun, Achieving the synergy of superior damage tolerance and oxidation resistance of 2D C_f/ZrB_2-SiC composites via fiber heat treatment, *Applied Surface Science*, 2021, **556**, 149807, doi: 10.1016/j.apsusc.2021.149807.

[7] C. Fang, P. Hu, S. Dong, P. Xie, K. Wang, X. Zhang, Design and optimization of the coating thickness on chopped carbon fibers and sintering temperature for ZrB_2-SiC-C_f composites prepared by hot pressing, *Journal of the European Ceramic Society*, 2019, **39**, 2805-2811, doi: 10.1016/j.jeurceramsoc.2019.03.038.

[8] H.J. Wang, P.Z. Gao, Z.H. Jin, Preparation and oxidation behavior of three-dimensional braided carbon fiber coated by SiC, *Materials Letters*, 2005, **59**, 486-490, doi: 10.1016/j.matlet.2004.10.028.

[9] M. Leparoux, L. Vandenbulcke, C. Clinard, Influence of Isothermal Chemical Vapor Deposition and Chemical Vapor Infiltration Conditions on the Deposition Kinetics and Structure of Boron Nitride, *Journal of the American Ceramic Society*, 2004, **82**, 1187-1195, doi: 10.1111/j.1151-2916.1999.tb01894.x.

[10] D. Zhang, P. Hu, S. Dong, Q. Qu, X. Zhang, Effect of pyrolytic carbon coating on the microstructure and fracture behavior of the C_f/ZrB_2-SiC composite, *Ceramics International*, 2018, **44**, 19612-19618, doi: 10.1016/j.ceramint.2018.07.210.

[11] Y. Cheng, P. Hu, W. Zhang, C. Ma, J. Feng, Q. Fan, X. Zhang, S. Du, One-step introduction of ZrC-SiC inside carbon fabric to fabricate high homogeneous and damage-tolerant composite inspired by vibration, *Journal of the European Ceramic Society*, 2019, **39**, 2251-2256, doi: 10.1016/j.jeurceramsoc.2019.02.030.

[12] B. Du, Y. Cheng, L. Xun, S. Zhang, J. Tong, Q. Lv, S. Zhou,

P. Hu, X. Zhang, Using PyC modified 3D carbon fiber to reinforce UHTC under low temperature sintering without pressure, *Journal of Advanced Ceramics*, 2021, **10**: 871-884, doi: 10.1007/s40145-021-0495-9.
[13] T. Zhang, L. Qi, S. Li, X. Chao, W. Tian, J. Zhou, Evaluation of the effect of PyC coating thickness on the mechanical properties of T700 carbon fiber tows, *Applied Surface Science*, 2019, **463**, 310-321, doi: 10.1016/j.apsusc.2018.08.195.
[14] X. Xi, Y. Chen, J. Wang, Y. Li, X. Shao, L. He, Q. Huang, X. Pei, A multiscale hydrothermal carbon layer modified carbon fiber for composite fabrication, *RSC Advances*, 2018, **8**, 23339-23347, doi: 10.1039/c8ra04064h.
[15] C. Fang, P. Hu, S. Dong, J. Song, X. Zhang, An efficient hydrothermal transformation approach for construction of controllable carbon coating on carbon fiber from renewable carbohydrate, *Applied Surface Science*, 2019, **491**, 478-487, doi: 10.1016/j.apsusc.2019.06.186.
[16] C. Fang, Y. Bao, P. Hu, S. Dong, D. Liu, H. Wang, X. Zhang, Effects of multilayer hydrothermal carbon interphases on mechanical properties and thermal shock resistance of CF/ZrB_2-SiCBN, *Journal of the European Ceramic Society*, 2022, **42**, 4759-4769, doi: 10.1016/j.jeurceramsoc.2022.05.029.
[17] H. Yang, C. Fang, H. Xu, X. Zhang, Y. Liu, J. Zhao, A. Wang, H. Lu, H. Wang, Shrinkage-controlled hydrothermal carbon: An advanced interphase for achieving synergistic stress dispersion and load transfer in C_f/ZrB_2-SiC composites, *Ceramics International*, 2025, **51**, 5085-5094, doi: 10.1016/j.ceramint.2024.11.482.
[18] J. Sun, B. Bhushan, Hierarchical structure and mechanical properties of nacre: a review, *RSC Advances*, 2012, **2**, 7617-7632, doi: 10.1039/c2ra20218b.
[19] J. Sun, J. Tong, Fracture toughness properties of three different biomaterials measured by nanoindentation, *Journal of Bionic Engineering*, 2007, **4**, 11-17, doi: 10.1016/s1672-6529(07)60007-9.
[20] A. G. Checa, J. H. E. Cartwright, M. G. Willinger, Mineral bridges in nacre, *Journal of Structural Biology*, 2011, **176**, 330-339, doi: 10.1016/j.jsb.2011.09.011.
[21] A.Y. M. Lin, P. Chen, M. A. Meyers, The growth of nacre in the abalone shell, *Acta Biomaterialia*, 2008, **4**, 131-138, doi: 10.1016/j.actbio.2007.05.005.
[22] N. Song, H. Pan, X. Hou, S. Cui, L. Shi, P. Ding, Enhancement of thermal conductivity in polyamide-6/graphene composites via a “bridge effect” of silicon carbide whiskers, *RSC Advances*, 2017, **7**, 46306-46312, doi: 10.1039/c7ra09094c.
[23] Y. Fang, A. Wang, K. He, H. Pan, J. Liao, Z. Ding, F. Xing, H. Le, X. Wang, Property evolution of geopolymer composites with SiC whiskers loaded with BN coating at elevated temperatures, *Construction and Building Materials*, 2021, **309**, 125130, doi: 10.1016/j.conbuildmat.2021.125130.
[24] L. Lai, Y. Bi, B. Niu, G. Yu, Y. Li, G. Ding, Q. Xu, Reinforcement mechanisms and current research status of silicon carbide whisker-reinforced composites: A comprehensive review, *Reviews on Advanced Materials Science*, 2024, **63**, 20240047, doi: 10.1515/rams-2024-0047.
[25] Z. Wang, C. Hong, X. Zhang, X. Sun, J. Han, Microstructure and thermal shock behavior of ZrB_2–SiC–graphite composite, *Materials Chemistry and Physics*, 2009, **113**, 338-341, doi: 10.1016/j.matchemphys.2008.07.095.
[26] A. K. Naik, S. Maharana, L. Bichler, T. Laha, S. Roy, Study of the influence of ZrB_2 content and thermal shock on the elastic modulus of spark plasma sintered ZrB_2-B_4C composites using a non-destructive ultrasonic technique, *Journal of the European Ceramic Society*, 2024, **44**, 679-692, doi: 10.1016/j.jeurceramsoc.2023.09.065.
[27] J. Zhou, B. Zhu, W. Zhao, Y. Zhang, J. Li, J. Fan, K. Qiao, Enhancement of interfacial performance of carbon fiber reinforced polypropylene composites by dual action of polyetherimide nanoparticles and coatings, *Colloids and Surfaces A: Physicochemical and Engineering Aspects*, 2024, **689**, 133776, doi: 10.1016/j.colsurfa.2024.133776.
[28] Y. Chai, H. Zhang, X. Zhou, Mechanical properties of SiC_f/SiC composites with alternating PyC/BN multilayer interfaces, *Advances in Applied Ceramics*, 2017, **116**, 392-399, doi: 10.1080/17436753.2017.1339517.
[29] H. Yu, X. Zhou, W. Zhang, H. Peng, C. Zhang, Mechanical behavior of SiC_f/SiC composites with alternating PyC/SiC multilayer interphases, *Materials & Design*, 2013, **44**, 320-324, doi: 10.1016/j.matdes.2012.07.073.
[30] Y. Cheng, Y. Zhang, F. Zhang, Y. Han, Y. Zhang, Y. An, C. Huang, L. Zhao, N. Hu, Using flexible hydrothermal carbon-coated continuous carbon fiber to fabricate C_f/ZrB_2-SiC composites by fused deposition modeling and precursor infiltration pyrolysis, *Journal of the European Ceramic Society*, 2024, **44**, 721-728, doi: 10.1016/j.jeurceramsoc.2023.09.055.
[31] C. Fang, P. Hu, S. Dong, J. Feng, L. Xun, X. Zhang, Influence of hydrothermal carbon coating on the properties of CF/ZrB_2/SiBCN prepared by slurry injection, *Journal of the European Ceramic Society*, 2021, **41**, 84-91, doi: 10.1016/j.jeurceramsoc.2020.08.019.
[32] Y. An, K. Wan, Y. Yang, Y. Jia, Y. Cheng, Fabrication method and mechanical properties of biomimetic C_f/ZrB_2-SiC ceramic composites with bouligand structures, *Journal of the European Ceramic Society*, 2023, **43**, 283-290, doi: 10.1016/j.jeurceramsoc.2022.10.017.
[33] L. Yang, L. Yin, C. Hong, S. Dong, C. Liu, X. Zhang, Strong and thermostable hydrothermal carbon coated 3D needled carbon fiber reinforced silicon-boron carbonitride composites with broadband and tunable high-performance microwave absorption, *Journal of Colloid and Interface Science*, 2021, **582**, 270-282, doi: 10.1016/j.jcis.2020.08.030.
[34] L. Zhang, C. Wei, S. Li, G. Wen, Y. Liu, P. Wang, Mechanical and thermal shock properties of laminated ZrB_2-SiC/SiC_w ceramics, *Ceramics International*, 2019, **45**, 6503-6508, doi: 10.1016/j.ceramint.2018.12.140.
[35] S. Li, C. Wei, W. Wang, P. Wang, Y. Liu, S. Li, G. Wen, Fracture toughness and R-curve behavior of laminated ZrB_2–SiC/SiC_w ceramic, *Journal of Alloys and Compounds*, 2019, **784**, 96-101, doi: 10.1016/j.jallcom.2018.12.304.
[36] T. Lei, Q. Ge, Y. Zhou, S. Wang, Microstructure and fracture

behavior of an Al_2O_3-ZrO_2-SiC_w ceramic composite, *Ceramics International*, 1994, **20**, 91-97, doi: 10.1016/0272-8842(94)90064-7.
[37] Y. Zhou, W. Zhu, T. Lei, Mechanical properties and toughening mechanisms of SiC_w/ZrO_2 (6% mol Y_2O_3) ceramic composites, *Ceramics International*, 1992, **18**, 141-145, doi: 10.1016/0272-8842(92)90087-t.
[38] Y. Yang, T. Zhu, N. Sun, X. Liang, Y. Li, H. Wang, Z. Xie, S. Sang, J. Dai, Mechanical and tribological properties of SiC whisker-reinforced SiC composites via oscillatory pressure sintering, *International Journal of Applied Ceramic Technology*, 2023, **20**, 2499-2510, doi: 10.1111/ijac.14374.
[39] T. Yan, M. Luo, J. Chen, H. Zhu, J. Chai, L. Niu, B. Chen, Y. Zhu, T. Shen, Microstructure and mechanical properties of high entropy $(MoTaTiVW)C_5$ ceramics toughened with silicon carbide whisker, *Ceramics International*, 2024, **50**, 15840-15847, doi: 10.1016/j.ceramint.2024.02.063.
[40] G. Shi, J. Song, Z. Wu, SiC_w-Al_2O_3-epoxy composites with enhanced 3D interlocking skeleton, *Materials Letters*, 2021, **283**, 128913, doi: 10.1016/j.matlet.2020.128913.
[41] G. Geng, X. Ma, H. Geng, Y. Wu, Effect of Thermal Cycles on the Thermal Expansion Behavior of T700 Carbon Fiber Bundles, *Chemical Research in Chinese Universities*, 2018, **34**, 451-456, doi: 10.1007/s40242-018-7430-9.
[42] J. W. Zimmermann, G. E. Hilmas, W. G. Fahrenholtz, R. B. Dinwiddie, W. D. Porter, H. Wang, Thermophysical Properties of ZrB_2 and ZrB_2–SiC Ceramics, *Journal of the American Ceramic Society*, 2008, **91**, 1405-1411, doi: 10.1111/j.1551-2916.2008.02268.x.